[^{3}H]Benzophenone Photolabeling Identifies State-Dependent Changes in Nicotinic Acetylcholine Receptor Structure†

Galo Garcia, III, David C. Chiara, Selvanayagam Nirthanan, Ayman K. Hamouda, Deirdre S. Stewart, and Jonathan B. Cohen*

Department of Neurobiology, Harvard Medical School, Boston, Massachusetts 02115

Received April 30, 2007; Revised Manuscript Received June 25, 2007

ABSTRACT: Interactions of benzophenone (BP) with the *Torpedo* nicotinic acetylcholine receptor (nAChR) were characterized by electrophysiological analyses, radioligand binding assays, and photolabeling of nAChR-rich membranes with [^{3}H]BP to identify the amino acids contributing to its binding sites. BP acted as a low potency noncompetitive antagonist, reversibly inhibiting the ACh responses of nAChRs expressed in *Xenopus* oocytes (IC_{50} = 600 μM) and the binding of the noncompetitive antagonist [^{3}H]-tetracaine to nAChR-rich membranes (IC_{50} = 150 μM). UV irradiation at 365 nm resulted in covalent incorporation of [^{3}H]BP into the nAChR subunits ($\delta > \alpha \sim \beta > \gamma$), with photoincorporation limited to the nAChR transmembrane domain. Comparison of nAChR photolabeling in the closed state (absence of agonist) and desensitized state (equilibrated with agonist) revealed selective desensitized state labeling in the δ subunit of δPhe-232 in δM1 and δPro-286/δIle-288 near the beginning of δM3 that are within a pocket at the interface between the transmembrane and extracellular domains. There was labeling in the closed state within the ion channel at position M2-13 (αVal-255, βVal-261, and δVal-269) that was reduced by 90% upon desensitization and labeling in the transmembrane M3 helices of the β and γ subunits (βMet-285, βMet-288, and γMet-291) that was reduced by 50−80% in the desensitized state. Labeling at the lipid interface (αMet-415 in αM4) was unaffected by agonist. These results provide a further definition of the regions in the nAChR transmembrane domain that differ in structure between the closed and desensitized states.

The nicotinic acetylcholine receptor (nAChR)[1] is a member of a superfamily of neurotransmitter-gated ion channels that also includes the serotonin 5-HT_3, $GABA_A$, and glycine receptors (*1*−*3*). Each receptor is composed of a pentamer of homologous subunits that associate at a central axis that is the ion channel. Information about the three-dimensional structure of these receptors is based primarily upon the crystal structures of soluble molluscan acetylcholine binding proteins, which are homologous to the extracellular domain of a homopentameric nAChR (*4*−*6*), and a model of the muscle-type nAChR (*7, 8*), built from 4 Å resolution electron density maps derived from cryoelectron microscope images of the *Torpedo* nAChR. Each receptor contains two transmitter binding sites located in the extracellular domain at subunit interfaces ($\alpha-\gamma$ and $\alpha-\delta$ for the *Torpedo* nAChR with an $\alpha_2\beta\gamma\delta$ subunit stoichiometry). The N-terminal half of each subunit contributes to the extracellular domain, and each subunit's transmembrane domain is made up of a loose bundle of four α helices (M1−M4), with M2 from each subunit forming the wall of the ion channel and M4 located most peripheral and in greatest contact with lipid. In addition to the direct primary structure link between the extracellular domain and M1 (preM1), within each subunit contact between the extracellular (ligand binding) and transmembrane (ion channel) domains is limited to a few amino acids in three loops at the base of the extracellular domain and approximately four amino acids between the C-terminus of M2 and the N-terminus of M3 (M2−M3 loop).

In the absence of agonist, nAChRs exist predominately in a resting, closed channel, conformation with low affinity for ACh. Agonist binding induces a series of conformational transitions leading transiently to an open channel state and then to a desensitized state that has the highest affinity for agonist and a nonconducting ion channel. Mutational analyses have identified state-dependent changes in structure in the ion channel (*9*) and interactions between amino acids at the base of the extracellular domain, pre-M1, and the M2−M3 loop that are important for agonist gating of the ion channel (*10*−*13*). Analyses of rate−equilibrium free energy relations for nAChR with single amino acid substitutions at positions in the extracellular or transmembrane domains suggest that gating occurs as a "conformational wave"

† This research was supported in part by U.S. Public Health Service Grant GM-58448 and by an award to Harvard Medical School from the Howard Hughes Biomedical Research Support Program for Medical Schools. G.G. was supported in part by a Merck Summer Undergraduate Research Fellowship, and S.N. was supported by a Brooks Foundation Fellowship in Neurobiology.

* To whom correspondence should be addressed. Tel: 617-432-1728. Fax: 617-734-7557. E-mail: jonathan_cohen@hms.harvard.edu.

[1] Abbreviations: nAChR, nicotinic acetylcholine receptor; Carb, carbamylcholine chloride; BP, benzophenone; V8 protease, *Staphylococcus aureus* endopeptidase Glu-C; EndoLys-C, endoproteinase Lys-C; OPA, *o*-phthalaldehyde; PCP, phencyclidine; TFA, trifluoroacetic acid; SDS, sodium dodecyl sulfate; PAGE, polyacrylamide gel electrophoresis; HPLC, high-pressure liquid chromatography; TPS, *Torpedo* physiological saline.

10.1021/bi7008163 CCC: $37.00
Published on Web 08/09/2007

propagating from the transmitter binding site to the ion channel (*14*, *15*).

Photolabeling the nAChR with uncharged, hydrophobic probes has provided an alternative method to identify changes in structure of the ion channel between closed and desensitized states (*16*, *17*) and, by photolabeling nAChRs frozen in the open state, to identify a structural change in the δ subunit transmembrane helix bundle that occurs upon channel opening (*18*) (see ref *19* for review). In addition, these probes identified nAChR amino acids at the lipid interface and provided evidence of the α-helical secondary structure of the M3 and M4 segments from the periodicity of labeling (*17*, *20*). The probes initially used, 3-(trifluoromethyl)-3-(*m*-iodophenyl)diazirine ([^{125}I]TID) and [^{3}H]diazofluorene, incorporate via carbene intermediates that react efficiently with water as well as amino acid side chains, which could limit their usefulness as structural probes in the presence of water.

In this report we characterize photolabeling of nAChRs in the closed and desensitized states with another hydrophobic photoprobe, [^{3}H]benzophenone (BP). In contrast to TID and diazofluorene, BP reacts via a ketyl diradical that will not react with water but can insert into C−H bonds with broad side-chain reactivity (reviewed in refs *21*−*23*), although reaction with methionine often dominates (*24*−*26*). That it does not react with water may make BP well-suited to probe the nAChR structure at the interface between the extracellular and transmembrane domains, a region likely to include both hydrophobic surfaces and water. Recently, when nAChRs expressed in *Xenopus* oocytes were photolabeled with BP (and hydrophobic derivatives of TID), LC/MS analyses indicated state-dependent labeling in the nAChR extracellular domain (*27*). We report here that when [^{3}H]-BP photolabels *Torpedo* nAChR-rich membranes, photolabeling is restricted to the transmembrane domain, with state-dependent labeling in the ion channel, in the δ subunit four-helix bundle, and at the $\beta-\alpha$ and $\gamma-\alpha$ subunit interfaces, as well as state-independent labeling at the lipid interface in αM4.

EXPERIMENTAL PROCEDUES

Materials. nAChR-enriched membranes were isolated from freshly dissected *Torpedo californica* electric organs as described (*28*) and stored at −80 °C in 38% sucrose and 0.02% sodium azide. [^{3}H]Benzophenone [4,4′-^{3}H] (50 Ci/mmol) was purchased from American Radiolabeled Chemicals, [^{3}H]tetracaine (30 Ci/mmol) from Sibtech, and [^{3}H]-phencyclidine [[^{3}H]PCP (27 Ci/mmol)] from Perkin-Elmer Life Science. [^{3}H]ACh (1.9 Ci/mmol) was a gift from Dr. Shaukat Husain (Massachusetts General Hospital). BP, carbamylcholine chloride (Carb), and the hydrochloride salts of tetracaine, proadifen, and PCP were from Sigma Chemical Co. *o*-Phthalaldehyde was from Pierce, 10% Genapol C-100 from Calbiochem, *Staphylococcus aureus* glutamyl endopeptidase Glu-C (V8 protease) from ICN Biomedical, and endoproteinase Lys-C (EndoLys-C) from Roche Applied Sciences. TPCK-treated trypsin was from Worthington.

Electrophysiology. The effects of BP on agonist-induced responses of wild-type *Torpedo* nAChRs expressed in *Xenopus* oocytes were measured by standard two-electrode voltage clamp as described (*29*). BP was prepared at 0.2 M in methanol and diluted into low-calcium ND96 recording solution (96 mM NaCl, 2 mM KCl, 0.3 mM $CaCl_2$, 1 mM $MgCl_2$, and 5 mM HEPES, pH 7.6) containing 1 μM atropine.

Radioligand Binding Assays. A centrifugation assay (*30*) was used to determine the equilibrium binding of [^{3}H]ACh, [^{3}H]tetracaine, or [^{3}H]PCP, in the absence or presence of 1 mM Carb, to nAChR-rich membranes in phosphate-buffered *Torpedo* physiological saline (TPS: 250 mM NaCl, 5 mM KCl, 3 mM $CaCl_2$, 2 mM $MgCl_2$, and 5 mM sodium phosphate, pH 7.0). For [^{3}H]tetracaine (9 nM) and [^{3}H]PCP (6 nM), 0.2 mL aliquots at 0.7 mg of protein/mL (∼500 nM ACh binding sites) were incubated with the drugs for 2 h before centrifugation at 15000 rpm in a microcentrifuge for 40 min. For [^{3}H]ACh, membrane suspensions were pretreated with diisopropyl phosphofluoridate (∼0.5 mM) to inhibit acetylcholinesterase activity; then [^{3}H]ACh (15 nM) and drugs were equilibrated with dilute membrane suspensions (1 mL, 40 nM ACh binding sites, ∼80 μg of protein/mL) for 30 min before centrifugation. Nonspecific binding was determined in the presence of 1 mM Carb for [^{3}H]ACh, 0.2 mM tetracaine for [^{3}H]tetracaine, and for [^{3}H]PCP in the presence of 1 mM proadifen (+Carb) or 1 mM tetracaine (−Carb). The averages of duplicate determinations were normalized to the binding determined in the absence of BP. With BP prepared as a 200 mM stock solution in methanol, at the highest concentration tested, the final concentration of methanol was 0.5% (v/v). Control experiments established 0.5% methanol altered by <5% the binding of [^{3}H]ACh or [^{3}H]PCP (or the ACh response for oocyte-expressed nAChR). For [^{3}H]tetracaine binding, the BP stock was in ethanol, with a final concentration of 1% ethanol at all BP concentrations tested.

Data Analysis. The concentration dependence of BP inhibition of ACh responses or radioligand binding was fit to the single site binding equation:

$$f_x = f_0/(1 + x/\mathrm{IC}_{50})$$

where f_x is the current or specific ^{3}H-labeled radioligand bound in the presence of BP at concentration x, f_0 is the current or specific radioligand bound in the absence of BP, and IC_{50} is the total inhibitor concentration associated with 50% inhibition of the ACh response or radioligand binding. Sigmaplot (SPSS) was used for the nonlinear least-squares fit of the data, and the standard errors of the parameter fits are indicated.

Photolabeling of nAChR-Rich Membranes with [^{3}H]BP. Membranes were photolabeled with [^{3}H]BP at low concentrations (0.2−0.8 μM) that were sufficient to incorporate enough ^{3}H into nAChR subunits to allow identification of labeled amino acids while minimizing the amount of ^{3}H required for each preparative photolabeling (∼100 μCi per sample). Freshly thawed nAChR-rich membranes (2 nmol of ACh sites/mg of protein) were diluted with TPS and pelleted, and the pellets, resuspended in TPS, were added to a glass vial containing the desired amount of solvent-free [^{3}H]BP. After equilibration with [^{3}H]BP for 20 min at 4 °C, aliquots of the membrane suspensions were added to other drugs in TPS (2 mg of protein/mL final concentration) and incubated for another 20 min. The membrane suspensions

were then transferred to a 96-well plastic microtiter plate (Falcon catalog no. 353911) for analytical-scale photolabelings (300 μg aliquots) or to 6 cm polystyrene Petri dishes (Falcon 1007) for preparative-scale labelings (10 mg of protein). The membrane suspensions, on ice, were irradiated with 365 nm UV light for 1 h in a Rayonet RPR-200 photochemical reactor (Southern New England Ultraviolet) using RPR-3500 bulbs. In analytical-scale photolabelings, after irradiation the suspensions were diluted with 2× sample buffer and then fractionated by SDS−PAGE, while preparative samples were pelleted and the pellets solubilized in 1× sample buffer.

Gel Electrophoresis and Proteolytic Digestions. SDS−PAGE was performed as described (*31*) using a modified Laemmli buffer system and 1.5 mm thick, 8% acrylamide gels. In analytical-scale labelings, polypeptides were visualized by Coomassie blue stain, and the gel was either prepared for fluorography (Amplify; Amersham Bioscience) and exposed to film (Kodak X-Omat) for 1−3 weeks at −80 °C or polypeptide bands were excised from the stained gel and ^{3}H incorporation was determined by scintillation counting (*28*). In preparative-scale experiments, the gels were stained with GelCode Blue stain reagent (Pierce). The nAChR β, γ, and δ subunits were isolated from the excised gel bands by passive elution into 12 mL of gel elution buffer (0.1 M NH_4HCO_3, 0.1% SDS, and 2.5 mM dithiothreitol, pH 8.4), while the α subunit was excised and placed in the well of a 15 cm long, 15% acrylamide gel for limited "in gel" digestion with V8 protease (200 μg) (*31*). The mapping gel was stained, and the α subunit proteolytic fragments of 20 kDa (αV8-20), 18 kDa (αV8-18), and 10 kDa (αV8-10) were eluted from the gel bands. Eluates were filtered (0.45 μm cellulose acetate membrane) and concentrated to <400 μL by centrifugal filtration (Vivaspin 15 M_r 5000 concentrators; Vivascience, Edgewood, NY). Subunits or subunit fragments were precipitated with 75% acetone (−20 °C, overnight) and then resuspended in 200 μL of resuspension buffer (15 mM Tris, 0.5 mM EDTA, pH 8.1, and 0.1% SDS). Based upon the MicroBCA protein assay (Peirce), 200−300 μg of nAChR β, γ, and δ subunits and 20−40 μg of αV-20, αV8-18, and αV8-10 were isolated from 10 mg of membranes.

For digestion with EndoLys-C, ∼150 μg of δ subunit or 20 μg of αV8-20 was combined with 0.5−0.75 unit of enzyme (3 units in 0.1 mL of water) and incubated for 14 days. Aliquots of the β, γ, and δ subunits in resuspension buffer were digested for 1 day at 25 °C with V8 protease (100% w/w). For digestion with trypsin (100% w/w), aliquots of the β subunit or αV8-10 were diluted 5-fold with digestion buffer (50 mM NH_4HCO_3 and 0.5% Genapol C-100, pH 8.1) and combined with 0.1 volume of trypsin in 20 mM $CaCl_2$ for digestion at 25 °C for 1 day. The proteolytic fragments from the β subunit trypsin digests and the δ subunit EndoLys-C digests were fractionated on 1.5 mm thick Tricine SDS−PAGE gels (*20*, *32*), while the other digests were fractionated directly by HPLC.

Reversed-Phase HPLC Purification. HPLC fractionation was carried out at 40 °C on an Agilent 1100 binary HPLC system on a Brownlee Aquapore butyl 7 μm column (100 × 2.1 mm) with a C-2 guard column with absorption monitored at 214 nm. Solvent A was 0.08% trifluoroacetic acid (TFA), and solvent B was 0.05% TFA in 60% acetonitrile and 40% 2-propanol. The flow rate was 0.2 mL/min, 500 μL fractions were collected, and the gradient used is shown in Figures 4B and 5A as dashed lines.

Sequence Analysis. Material for sequence analysis was isolated from four independent preparative photolabelings: Ia/b (control vs tetracaine), IIa/b/c (control, +Carb, +Carb + proadifen), IIIa/b (control, +Carb), and IVa/b/c (control, +Carb, +Carb + phencyclidine). N-Terminal sequencing was performed on a Procise 492 sequencer (Applied Biosystems), which was modified such that one-sixth of each cycle was injected for PTH derivative quantitation and five-sixths was collected for ^{3}H counting. Samples were usually applied directly to TFA-treated glass fiber disks (AB no. 401111) pretreated with Biobrene, with HPLC fractions drop-loaded at 45 °C. Filters containing samples in 0.1% SDS were washed to remove detergent before sequencing by treatment with gas TFA (5 min) followed by consecutive washes with *n*-butyl chloride and ethyl acetate (4 min each). Since the αM4 or δM1 fragments were sequenced inefficiently on glass filters, these samples were immobilized on PVDF disks for sequencing at high repetitive yield. For these samples, pooled HPLC fractions were diluted with 2 volumes of 0.1% aqueous TFA (to reduce organic concentration) and loaded onto PVDF disks using Prosorb sample preparation cartridges (Applied Biosystems no. 401959). In some cases, the sequencing run was interrupted, and the material on the filter was treated with *o*-phthalaldehyde (OPA) as described previously (*28*). OPA reacts preferentially with primary rather than secondary amines (i.e., proline) and can be used at any cycle of Edman degradation to block sequencing of peptides not containing an N-terminal proline (*33*).

The amount of released PTH derivative in each cycle, which was determined by comparison to standards from the background-corrected peak height using the model 610A Data Analysis Program, is shown in the figures along with the ^{3}H released in each cycle. To determine the amount of peptide in each sample, the background-subtracted number of picomoles detected [$f(x)$] in cycle x was fit to the equation $f(x) = I_0R^x$, and the equation was solved for I_0 (initial peptide amount) and R (average repetitive yield). Ser, Cys, Arg, His, and Trp residues were excluded from the fit due to known problems with their quantitation. Unless otherwise noted, the efficiency of labeling of an amino acid [counts per minute (cpm) per picomole] was calculated as $(\mathrm{cpm}_x - \mathrm{cpm}_{x-1})/(5I_0R^x)$.

Molecular Modeling. Insight II (Accelrys, San Diego, CA) and PyMOL (DeLano Scientific LLC, Palo Alto, CA) molecular modeling programs were used to locate the amino acids photolabeled by BP within the model of the *Torpedo* nAChR structure in the absence of agonist [PDB code 2BG9 (*8*)]. Potential aqueous drug binding pockets within the nAChR transmembrane domain were determined using the program PASS (*34*) with default parameters. The Docking program (Insight II) was used to determine whether BP could be accommodated in the predicted pockets near the photolabeled amino acids. To create a visual representation of the docking results, in each of the pockets a Connolly surface representation was made from the combination of all of the docked BP molecules. With a potential binding site within the channel lumen defined by the channel-facing M2 residues spanning from M2-2 to M2-20, 45 distinct BP orientations were obtained that were each restricted within M2-6 to M2-

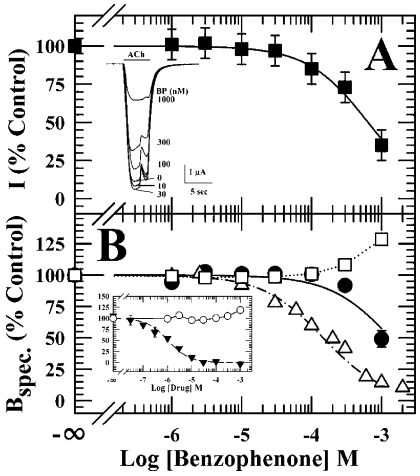

FIGURE 1: Interactions of BP with *Torpedo* nAChRs. (A) BP inhibition of nAChRs expressed in *Xenopus* oocytes. Oocytes were exposed for 5 s to 3 μM ACh in the absence or presence of the indicated concentrations of BP, and the peak currents in the presence of BP were normalized to the control current in the absence (insert). After exposure to 1 mM BP and washing for 3−5 min, ACh responses recovered to >90% of control. Data are means (±SD) from experiments on two oocytes. The IC_{50} was 640 ± 50 μM. (B) Effects of BP on the specific binding to nAChR-rich membranes of 10 nM [^{3}H]ACh (□), 9 nM [^{3}H]tetracaine (△), or 6 nM [^{3}H]-PCP in the presence of 1 mM Carb (●). Insert: Effects of tetracaine (▼) or BP (○) on the specific binding of 6 nM [^{3}H]PCP in the absence of Carb. For BP inhibition of [^{3}H]tetracaine binding, the IC_{50} was 150 ± 20 μM, and tetracaine inhibited [^{3}H]PCP binding with an IC_{50} of 1.1 ± 0.2 μM. For each radioligand, the data were normalized to the specific binding determined in the absence of BP, which for [^{3}H]ACh was 8520 ± 230 cpm. For [^{3}H]tetracaine it was 15600 ± 250 cpm, and for [^{3}H]PCP it was 5580 ± 150 cpm (+Carb) and 740 ± 40 cpm (−Carb). Nonspecific binding was 95 cpm for [^{3}H]ACh and 3080 ± 50 cpm for [^{3}H]tetracaine. For [^{3}H]-PCP it was 500 ± 50 cpm (+Carb) and 610 ± 30 cpm (−Carb).

13. For the pocket at the $\beta-\alpha$ or $\gamma-\alpha$ subunit interface, a BP molecule was placed initially within the pocket defined by PASS, and the potential binding site was defined as all residues within 8 Å of this molecule. For each interface docking study, 30 distinct BP orientations were obtained. For docking within the δ subunit helical bundle, a BP molecule was placed within the pocket defined by the PASS program, with the potential binding site defined as all residues within 8 Å and the residues labeled in this region by BP in the desensitized state or by TID in the open state (*18*). Thirteen distinct BP orientations were identified, two of which were nearly identical, wedged between δPhe-232 and δTyr-228, and obtained in 55 of the 103 successful minimizations.

RESULTS

Benzophenone, a Low Potency nAChR Antagonist. Interactions of BP with the *Torpedo* nAChR were characterized electrophysiologically by measuring the responses of nAChRs expressed in *Xenopus* oocytes (Figure 1A) and biochemically by measuring the equilibrium binding to nAChR-rich membranes of [^{3}H]ACh and drugs that bind in the ion channel preferentially in the resting state ([^{3}H]tetracaine) (*35*) or the desensitized state [[^{3}H]phencyclidine (PCP)] (*36*) (Figure 1B). BP at concentrations up to 1 mM produced no detectable nAChR current response. When coapplied with ACh, BP produced a reversible, concentration-dependent inhibition of ACh-induced currents characterized by an IC_{50} of 640 μM.

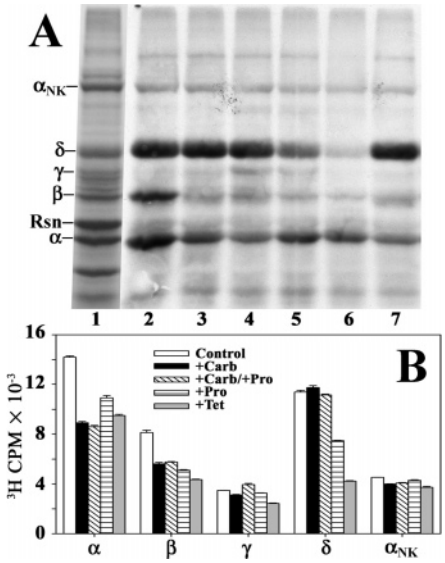

FIGURE 2: Photoincorporation of [^{3}H]BP into *Torpedo* nAChR-rich membranes. Membrane suspensions (300 μg aliquots at 2 mg/mL) were equilibrated with 0.8 μM [^{3}H]BP alone (lane 2) or with 2 mM Carb (lane 3), 2 mM Carb and 0.1 mM proadifen (lane 4), 0.1 mM proadifen (lane 5), 0.1 mM tetracaine (lane 6), or 2 mM Carb and 0.1 mM PCP (lane 7). After 1 h irradiation at 365 nm, the samples were subjected to SDS−PAGE, and the gel was visualized by Coomassie blue stain (A, lane 1) and prepared for fluorography (A, lanes 2−7, 30 day exposure). Indicated on the left are the mobilities of the nAChR subunits, rapsyn (Rsn), and the α subunit of the Na^+/K^+-ATPase (α_{NK}). (B) ^{3}H incorporation in the excised gel bands, as detemined by liquid scintillation counting.

In the absence of agonist BP inhibited [^{3}H]tetracaine binding with an IC_{50} of 150 μM, but even at 1 mM it did not inhibit [^{3}H]PCP binding. In the presence of agonist BP at 1 mM inhibited [^{3}H]PCP binding by 50%. BP at 1 mM increased the binding of [^{3}H]ACh by 30%. Thus, BP acted as a nAChR noncompetitive antagonist, but of much lower potency than TID, another uncharged, hydrophobic drug which is known to inhibit nAChR responses, [^{3}H]tetracaine binding in the absence of agonist, and [^{3}H]PCP binding in the presence of agonist, all with an IC_{50} of ~3 μM, while having no effect on [^{3}H]PCP binding in the absence of agonist (*30*, *37*, *38*).

Photoincorporation of [^{3}H]BP into nAChR-Rich Membranes. SDS−PAGE was used to identify the pattern of nAChR subunit photolabeling for membranes equilibrated with [^{3}H]BP (0.8 μM) in the presence or absence of the agonist carbamylcholine (Carb) and/or other drugs that bind in the ion channel preferentially in the desensitized state [proadifen (*39*) and PCP] or the resting state [tetracaine (*38*)]. A fluorogram of a representative gel is shown in Figure 2A, and ^{3}H incorporation into nAChR subunits was quantified by liquid scintillation counting of excised gel bands (Figure 2B).

For membranes labeled in the absence of agonist, [^{3}H]BP photoincorporated primarily into the nAChR α, β, and δ subunits, with the labeling of δ at approximately twice the efficiency of α (for a nAChR subunit stoichiometry $\alpha_2\beta\gamma\delta$). Tetracaine inhibited subunit photolabeling by 35% (α) to 65% (δ), suggesting that some of the labeling of nAChR in the resting state might be within the ion channel. The 8000 cpm of tetracaine-inhibitable labeling in the δ subunit constituted specific labeling of ~0.2% of subunits at 0.8 μM [^{3}H]BP. In the presence of Carb (desensitized state), pho-

tolabeling of the α and *β* subunits was reduced by ~40%, while the *δ* subunit photolabeling was not reduced. The subunit photolabeling in the desensitized state was not inhibited by proadifen or PCP. The pharmacological specificity of labeling seen for the α and *β* subunits was qualitatively similar to that for [^{125}I]TID, for which Carb or tetracaine reduced labeling of all subunits by ~80% (*31*, *40*). However, the prominent labeling of the *δ* subunit in the presence of Carb, which was insensitive to both proadifen and PCP, was novel and, in conjunction with the tetracaine-inhibitable labeling in the closed state, suggested that in the *δ* subunit the labeling of amino acids contributing to the ion channel (*δ*M2) was less efficient in the desensitized than in the closed state and that there was additional, Carb-enhanced labeling elsewhere in the subunit.

Mapping [^{3}H]BP Photoincorporation into α and δ Subunit Proteolytic Fragments. To begin to identify the regions of subunit primary structure photolabeled by [^{3}H]BP, the nAChR-rich membranes were photolabeled in three conditions (−Carb, +Carb, and +Carb + proadifen), and the α and *δ* subunits were isolated and subjected to limited proteolytic fragmentation to generate large, nonoverlapping fragments containing either the extracellular or transmembrane domain. Digestion of the α subunit "in gel" with V8 protease generates fragments of 20 kDa (αV8-20), beginning at αSer-173 and containing ACh binding site segment C as well as the M1−M3 membrane spanning helices; 18 kDa (αV8-18), beginning at αThr-52 and containing ACh binding site segments A and B; and 10 kDa (αV8-10), beginning at αAsn-338 and containing αM4 (*31*). Digestion of the *δ* subunit in solution with EndoLys-C produces a fragment of ~21 kDa (*δ*EKC-21), beginning at *δ*His-20/*δ*Glu-48 and containing ACh binding site segments D, E, and F, and fragments of 10−14 kDa (*δ*EKC-10/14), one beginning at *δ*Met-257 at the N-terminus of *δ*M2 and extending through *δ*M3 and the other beginning at *δ*Phe-206 and containing a site of N-linked glycosylation at *δ*Asn-208 and *δ*M1 (*18*) (Figure 3). Within the α subunit, Carb-inhibitable labeling was restricted to αV8-20, where labeling was reduced by 50% in the presence of Carb. Within the *δ* subunit, in the presence of Carb, ^{3}H incorporation in *δ*EKC-10/14 was increased by 60%, and the enhanced labeling was inhibitable by proadifen. Although some ^{3}H was recovered from the gel bands containing αV8-18 and *δ*EKC-21, further purification by reversed-phase HPLC established that less than 10% of the ^{3}H in those bands was associated with αV8-18 or *δ*EKC-21, each of which eluted as a sharp peak at ~45% organic well resolved from a broad peak of ^{3}H eluting at >60% organic (Supporting Information Figure S1). On the basis of this analysis, less than 2% of [^{3}H]BP photoincorporation into the α or *δ* subunit photoincorporation was within αV8-18 or *δ*EKC-21, the fragments containing large portions of each subunit's extracellular domain.

Agonist-Inhibitable [^{3}H]BP Photolabeling in the M2 Ion Channel Domain. To identify the amino acids labeled in *δ*M2, *δ*EKC-10/14 was isolated by Tricine SDS−PAGE from EndoLys-C digests of labeled *δ* subunits (Figure 4A) and then further fractionated by reversed-phase HPLC (Figure 4B). For each labeling condition, the major peak of ^{3}H eluted at 65−70% organic, where the fragment beginning at *δ*Met-257 elutes (*18*), and for the +Carb sample, there was a minor ^{3}H peak eluting at 55% organic (fraction 23),

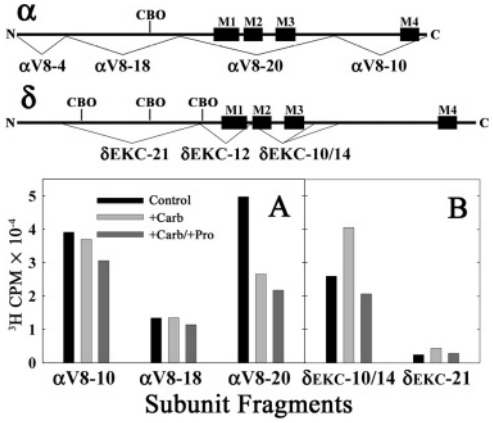

FIGURE 3: Mapping [^{3}H]BP incorporation into large fragments of the nAChR α and *δ* subunits. nAChR-rich membranes (10 mg of protein at 2 mg/mL) were photolabeled with 0.3 *μ*M [^{3}H]BP without other drugs (control), with 2 mM Carb, or with 2 mM Carb and 0.1 mM proadifen. After photolabeling, the membranes were subjected to SDS−PAGE, and the nAChR subunits were excised from the stained gel. Indicated in the diagrams above are the nAChR α subunit (upper) and *δ* subunit (lower) proteolytic fragments produced by digestion with V8 protease (*31*) and EndoLys-C (*18*), respectively. (A) The stained gel strips corresponding to the α subunits were transferred to the wells of a 15% acrylamide "mapping" gel and digested in gel with V8 protease. After electrophoresis and staining, the ^{3}H and polypeptides were eluted from the bands containing αV8-10, αV8-18, and αV8-20. When the material eluted from the gel band containing αV8-18 was further purified by reversed-phase HPLC, ~10% of ^{3}H was recovered in the fractions containing αV8-18 with the remainder eluting in a hydrophobic peak, consistent with elution properties of αV8-20 (Supporting Information Figure S1A). (B) The *δ* subunits were excised, eluted and concentrated, and then digested with EndoLys-C, and the digests were fractionated by Tricine gel SDS−PAGE. After electrophoresis the gel was cut into 1 cm bands and material eluted (Figure 4A). The peak of ^{3}H was in band 12, corresponding to *δ*EKC-10/14. *δ*EKC-21, which was identified by Coomassie blue stain, was in band 15 (Supporting Information Figure S1B). The ^{3}H eluted from the gel slices of a single experiment is plotted in (A) and (B). Upon the basis of the intensity of the Coomassie blue stain of the bands in the gel, there were similar amounts of each subunit fragment in the three labeling conditions.

where the fragment beginning at *δ*Phe-206 elutes. The ^{3}H peaks were larger for the sample from nAChRs labeled in the desensitized state than in the closed state. Sequence analysis of the major peak (Figure 4C) established the presence of a single fragment beginning at *δ*Met-257 with ^{3}H release in cycle 13 (−Carb, 1800 cpm), which was reduced by 80% in the +Carb sample (330 cpm) and by ~95% in the sample labeled in the presence of Carb and proadifen (70 cpm). On the basis of the levels of the *δ*M2 fragment in each sample, the observed ^{3}H releases indicated labeling of *δ*M2-13 (*δ*Val-269) at 90 cpm/pmol (−Carb), 20 cpm/pmol (+Carb), and 4 cpm/pmol (+Carb/+proadifen).

To further characterize the pharmacological specificity of [^{3}H]BP photoincorporation in the ion channel in the closed state, the fragment beginning at *δ*Met-257 was also isolated from nAChRs labeled in the absence and presence of tetracaine. Sequence analysis revealed labeling of *δ*M2-13 that was reduced by ~95% in the presence of tetracaine, as well as tetracaine-inhibitable labeling of *δ*M2-9 (*δ*Leu-265) at about 5% the efficiency of *δ*M2-13 (*δ*Val-269, Figure 4D).

The incorporation of [^{3}H]BP in αM2 and *β*M2 was also determined for nAChRs labeled in the absence and presence of Carb. The fragment beginning at αMet-243 at the

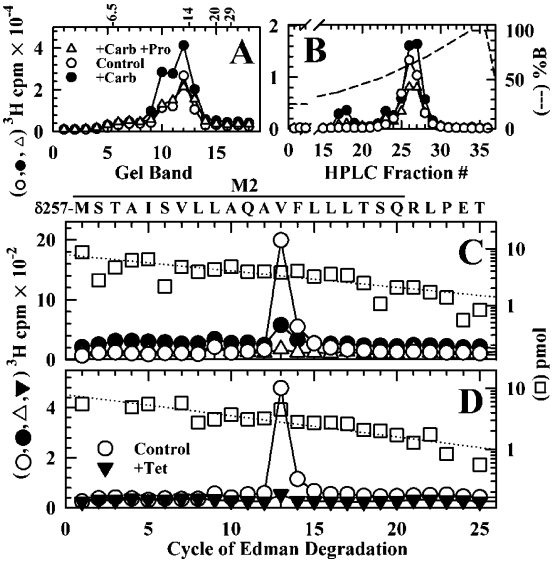

FIGURE 4: State-dependent [3H]BP photolabeling in the δM2 ion channel domain. δ subunits, isolated from nAChRs photolabeled with 0.3 μM [3H]BP in the absence of other drugs (○), in the presence of Carb (●), or in the presence of Carb and proadifen (△), were digested with EndoLys-C, and the digests were fractionated by Tricine gel SDS−PAGE. After electrophoresis, the gel lanes were cut into 1 cm bands, and material was eluted. (A) Distribution of 3H eluted from gel bands (cpm loaded: control, 73000 cpm; +Carb, 111000 cpm; +Carb + Pro, 65000 cpm). (B) 3H elution profile (○, ●, △) when the material from gel band 12 was purified by reversed-phase HPLC. Also plotted is the percent solvent B (− −). (C) 3H (○, ●, △) and PTH-amino acids released (□) when the HPLC peak of 3H (fractions 26 and 27) was sequenced. A single sequence was detected beginning at δMet-257, the N-terminus of δM2, with any other sequence at <5% that level [control, I_0 = 10 pmol (□); +Carb, I_0 = 9 pmol; +Carb + Pro, I_0 = 8 pmol]. The 3H release in cycle 13 in the absence of agonist (1800 cpm) was consistent with labeling of δVal-269 at 90 cpm/pmol, and that labeling was reduced to 20 cpm/pmol (+Carb) and 4 cpm/pmol (+Carb + Pro). (D) 3H (○, ▼) and PTH-amino acids released (□) during sequence analysis of δEKC-10/14 isolated from nAChRs labeled with 0.2 μM [3H]BP in the absence (○,(□) or presence (▼) of tetracaine (control, I_0 = 8 pmol; +Tet, I_0 = 6 pmol). The 3H release in cycle 13 (control, 440 cpm) indicated labeling of δVal-269 at 18 cpm/pmol that was reduced to 3 cpm/pmol (+Tet).

N-terminus of αM2 was purified by reversed-phase HPLC from an EndoLys-C digest of αV8-20 (Supporting Information Figure S3A) (*41*, *42*), while an ∼7 kDa fragment beginning at βMet-249 was isolated by Tricine SDS−PAGE and reversed-phase HPLC from a trypsin digest of the β subunit (Supporting Information Figure S2) (*38*).

When the HPLC fractions containing the peak of 3H from EndoLys-C digests of αV8-20 were sequenced (Figure 5A), the primary sequence began at αMet-243 (I_0 = 5 pmol), with secondary sequences beginning at αHis-186 (I_0 = 2 pmol) and at αTyr-277 (I_0 = 0.6 pmol), the N-terminus of αM3. In the resting state, the major release of 3H was in cycle 13 (110 cpm), corresponding to labeling of αM2-13 (αVal-255) at 12 cpm/pmol, and that labeling was reduced by ∼75% for nAChRs labeled in the desensitized state. There was also lower level 3H release in cycle 6 (30 cpm) for the samples labeled in the absence and presence of Carb. However, further studies will be required to determine whether the cycle 6 release results from state-independent labeling of αM2-6 at low efficiency (∼2 cpm/pmol) or from labeling of αMet-282 within αM3. Labeling of αMet-282 is more likely, since the equivalent methionines in the β and γ

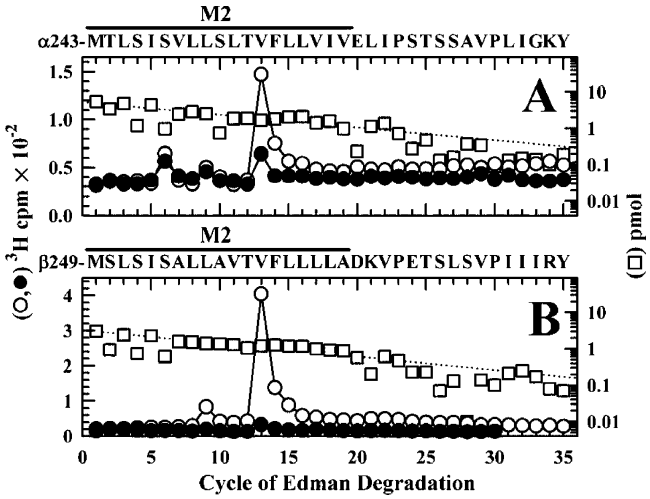

FIGURE 5: State-dependent [3H]BP photolabeling in αM2 (A) and βM2 (B). 3H (○, ●) and PTH-amino acids released (□) during sequencing of fragments isolated from the photolabeling experiment shown in Figure 4 from nAChRs labeled in the absence (○) or presence (●) of Carb. EndoLys-C digests of αV8-20 were fractionated by reversed-phase HPLC (Supporting Information Figure S3A), and fractions containing the peak of 3H were pooled for sequencing. Trypsin digests of β subunits were fractionated by Tricine gel SDS−PAGE (Supporting Information Figure S2A), and material eluted from an ∼7 kDa band, that contained the peak of 3H on the gel, was repurified by reversed-phase HPLC (Supporting Information Figure S2B) and sequenced. (A) The primary sequence began at αMet-242 (□, −Carb, I_0 = 5 pmol, +Carb, I_0 = 5 pmol), with secondary sequences beginning at αHis-186 (I_0 = 2 pmol) and αTyr-277, the N-terminus of αM3 (I_0 = 0.6 pmol). The 3H release in cycle 13 (115 cpm) indicated labeling of αVal-255 at 12 (−Carb) and 5 (+Carb) cpm/pmol. The 3H release in cycle 6 (30 cpm) may be associated with labeling of αMet-282 in the secondary sequence at ∼8 cpm/pmol (see text). (B) The primary sequence began at βMet-249 (□, −Carb, I_0 = 3 pmol, +Carb, I_0 = 2 pmol), with any secondary sequences at less than 10% that level. The 3H releases in cycles 9 (50 cpm) and 13 (370 cpm) were consistent with labeling of βLeu-257 and βVal-261 at 7 and 66 cpm/pmol that was reduced by 90% in the presence of Carb.

subunits are labeled (see later), and in sequence analyses of α subunit samples from several different labeling experiments, the 3H release in cycle 6 correlated better with the levels of the αM3 than the αM2 peptide.

For nAChRs labeled in the resting state, sequence analysis of the fragment beginning at βMet-249 (Figure 5B) was characterized by a peak of 3H release in cycle 13 (370 cpm) and lower level release in cycle 9 (50 cpm), consistent with labeling of βM2-13 (βVal-261) and βM2-9 (βLeu-257) at 70 and 6 cpm/pmol. The efficiency of labeling at each position was reduced by ∼90% when nAChRs were labeled in the desensitized state.

Agonist-Enhanced Labeling in the δM2−δM3 Loop and in δM1. The 3H cpm incorporated in δEKC-10/14 and in the HPLC fractions containing the fragment beginning at the N-terminus of δM2 (Figure 4A,B) were greater for nAChRs labeled in the desensitized state than the closed state, but the efficiency of [3H]BP incorporation in amino acids in δM2 in the desensitized state was only 20% of that in the closed state (Figure 4C). This suggested that, for nAChRs labeled in the desensitized state, there must be photolabeled amino acids elsewhere within the fragment, presumably in the M2/M3 loop and/or in δM3.

To investigate this, we used V8 protease to cleave the δ subunit at δGlu-280 near the C-terminus of δM2 (*20*) and

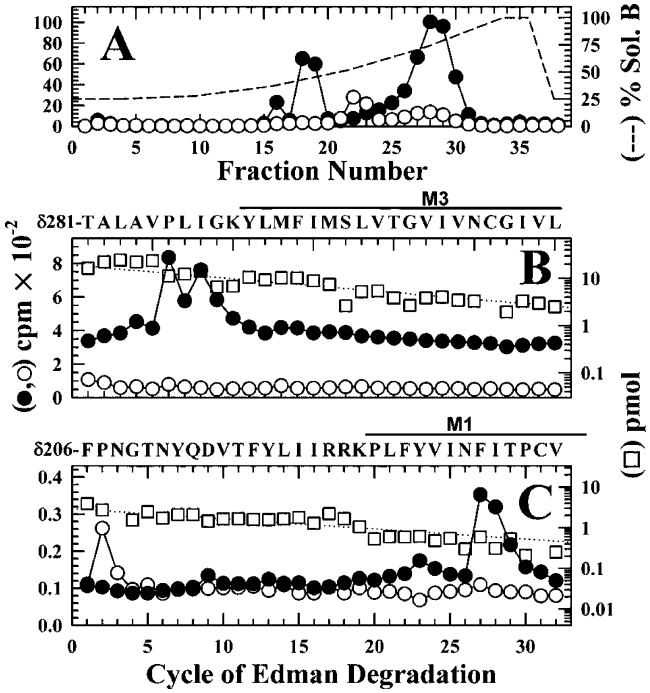

FIGURE 6: Agonist-enhanced [^{3}H]BP photolabeling in δM3 and δM1. ^{3}H (○, ●) and PTH-amino acids released (□) during sequencing of fragments isolated from V8 protease digests (B) and EndoLys-C digests (C) of δ subunits isolated from nAChRs labeled with [^{3}H]BP (0.3 μM) in the absence (○) or presence (●) of Carb. For this labeling, [^{3}H]BP photolabeled δVal-269 in δM2 at 40 (−Carb) and 7 (+Carb) cpm/pmol. (A) To identify labeling in δM3, V8 protease digests of labeled δ subunits were fractionated by reversed-phase HPLC (10% aliquots counted), and fractions 27−29, containing the peak of ^{3}H (~70% solvent B), were pooled and sequenced (B), with the samples treated with OPA at cycle 6 to prevent further sequencing of any peptide not containing a Pro at that cycle of Edman degradation. After OPA treatment, sequencing continued for the fragment beginning at δThr-281 [+Carb (□), I_0 = 19 pmol, R = 94%; −Carb, I_0 = 15 pmol, R = 92%]. In the cycles before OPA, sequences were also present that began at δIle-192 and δVal-443 (I_0's of 16 pmol). Treatment with OPA reduced those levels by >95%. The releases of ^{3}H in cycles 6 (420 cpm) and 8 (180 cpm) in the +Carb sample indicated labeling of δPro-286 and δIle-288 at 6 and 3 cpm/pmol, with labeling at those positions in the resting state (−Carb) at <10% those levels. (C) To identify labeling in δM1, δEKC-10/14 was isolated by SDS−PAGE and further purified by reversed-phase HPLC, as in Figure 4A,B, and the material in fractions 24 and 25, containing a shoulder of ^{3}H (~60% solvent B), was sequenced with OPA treatment at cycle 20. After OPA, sequencing continued for the fragment beginning at δPhe-206 [+Carb (□), I_0 = 3 pmol, R = 94%; −Carb, I_0 = 2 pmol, R = 94%]. The ^{3}H release in cycle 27 (+Carb, 22 cpm) indicated labeling of δPhe-232 at 7 cpm/pmol, with labeling in the resting state (−Carb) at <10% that level. The ^{3}H release seen in cycle 2 (−Carb, 16 cpm) was not seen in samples from two other independent photolabeling experiments, and its origin is unknown.

characterized labeling in the fragment beginning at δThr-281 by sequencing the material that eluted as a broad, hydrophobic peak of ^{3}H when the subunit digest was fractionated by reversed-phase HPLC (Figure 6A). To identify ^{3}H release from the fragment beginning at δThr-281, we took advantage of the presence of a proline (δPro-286) in the sixth cycle of Edman degradation and of a sequencing protocol in which *o*-phthalaldehyde (OPA), which reacts with primary amines but not proline, is applied prior to a cycle containing a proline to prevent Edman degradation of all peptides without an N-terminal proline (*28*, *33*). When aliquots of the peak of ^{3}H from the HPLC of theV8 digest were sequenced, fragments were identified in the initial cycles of Edman degradation beginning at δThr-281 (I_0 =19 pmol), δIle-192 (I_0 = 17 pmol), and δVal-443 (I_0 = 16 pmol). After treatment with OPA in cycle 6, sequencing of the δThr-281 fragment continued without reduction of repetitive yield, while the mass levels of the other peptides were reduced by >95%. For nAChRs labeled in the desensitized state, there were peaks of ^{3}H release in cycles 6 (420 cpm) and 8 (180 cpm), corresponding to the labeling of δPro-286 at 6 cpm/pmol[2] and δIle-288 at 3 cpm/pmol, while there was no ^{3}H release above background for the sample from nAChRs labeled in the resting state, despite the presence of the δThr-281 fragment at similar level (Figure 6B).

We also determined that there was Carb-enhanced labeling in δM1, primarily in δPhe-232, by sequencing material in the minor peak of ^{3}H that eluted at 55% organic in the HPLC fractionation of δEKC-10/14 (Figure 4B). The primary sequence began at δPhe-206 (I_0 = 3 pmol), and sequencing of that peptide continued after treatment with OPA in cycle 20 (δPro-226) (Figure 6C). For nAChRs labeled in the desensitized state, the ^{3}H release in cycle 27 (25 cpm) indicated labeling of δPhe-232 at 7 cpm/pmol,[3] while for nAChRs labeled in the closed state, the labeling at that position was reduced by ≥90%.

Agonist-Inhibitable [^{3}H]BP Labeling in βM3 and γM3. Within the δ-subunit there was prominent labeling in the δM2−M3 loop for nAChRs in the desensitized state, with no detectable labeling in δM3 in either the presence or absence of agonist. Since the V8 protease cleavage site (βGlu-272, γGlu-275, and δGlu-280) and the proline in the M2−M3 loop (βPro-278, γPro-281, and δPro-286) are conserved between the β, γ, and δ subunits (Figure 7), we used the same methodology to characterize [^{3}H]BP incorporation in the M2−M3 loop and M3 of the β and γ subunits: V8 protease digestion, HPLC fractionation, and sequence analysis with OPA treatment in cycle 6 (Figure 7). For β subunits isolated from nAChRs labeled in the absence of agonist, there were peaks of ^{3}H release in cycles 13 (45 cpm) and 16 (105 cpm), consistent with the labeling of the two methionines in βM3 (βMet-285 and βMet-288) at 2 and 5 cpm/pmol (Figure 7A). For the γ subunit, there was a ^{3}H peak in cycle 16 (75 cpm), consistent with labeling of γMet-291, one of three methionines in γM3, at 3 cpm/

[2] The efficiency of desensitized state labeling of δPro-286 is likely to be substantially higher than the 6 cpm/pmol calculated from the increased ^{3}H release in cycle 6, as we have observed that the BP adduct of δPro-286 is unstable under the acid treatments of standard sequencing conditions. This was evidenced by ^{3}H release when samples containing labeled δPro-286 were subjected to pulses of acid and by the high background release of ~250 cpm/cycle during sequence analysis of the fragment beginning at δMet-257 (+Carb) (Figure 4C). The instability of BP adducts of Pro has been reported previously (*21*, *45*).

[3] The efficiency of desensitized state labeling of δPhe-232 is substantially higher than the 7 cpm/pmol calculated from the increased ^{3}H release in cycle 27 (Figure 6B). We found evidence that the δ subunit fragments labeled at δPhe-232 were susceptible to cleavage at the C-terminus of labeled δPhe-232 with formation of more hydrophilic labeled fragments that elute in the HPLC at 35% solvent B (Figure 4B, fractions 17 and 18; Figure 6A, fractions 18 and 19). Such instability appears to be consistent with the report by Deseke et al. (*23*) that β carbon BP adducts of the Phe-OMe ester in an aqueous environment were recovered quantitatively as a cyclized lactone.

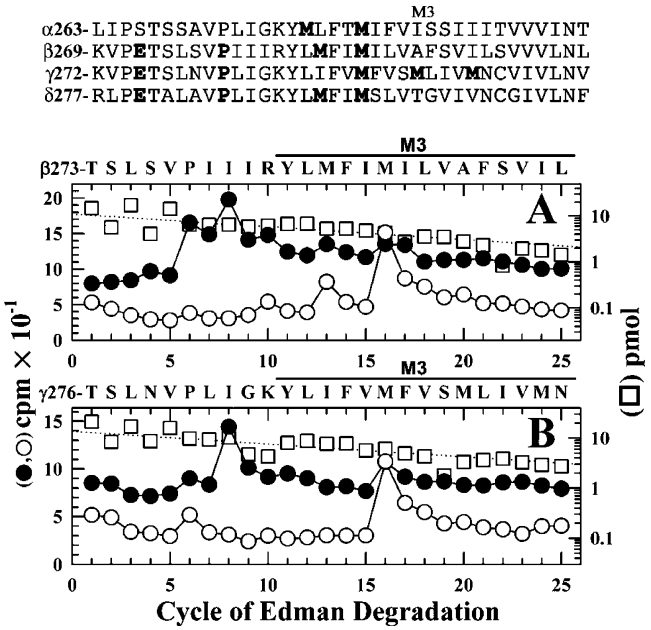

FIGURE 7: Agonist-sensitive [3H]BP photolabeling in βM3 and γM3. 3H (○, ●) and PTH-amino acids released (□) during sequencing of fragments from V8 protease digests of β and γ subunits isolated from the nAChRs, from the photolabeling experiment also used for Figure 6, labeled in the absence (○) or presence (●) of Carb. The V8 protease digests were fractionated by reversed-phase HPLC, and fractions containing the peak of 3H (~70% solvent B) were pooled and sequenced, with the samples treated with OPA at cycle 6. For the β subunit (A), after OPA, sequencing continued for the fragment beginning at βThr-273 [−Carb and +Carb (□), I_0 = 11 pmol, R = 94%] and for the equivalent, contaminating fragment from the δ subunit (δThr-281, I_0 = 3 pmol). For the γ subunit (B), the primary sequence began at γThr-276 [−Carb and +Carb (□), I_0 = 13 pmol, R = 94%], and there was the contaminating δ subunit fragment (δThr-281, I_0 = 3 pmol). Since no 3H release was seen for the −Carb δ subunit fragment (Figure 6A), the 3H releases in cycles 13 (β, 45 cpm) and 16 (β, 105 cpm; γ, 75 cpm) indicate labeling of βMet-285, βMet-288, and γMet-291 at 2, 5, and 3 cpm/pmol (−Carb) that was reduced to 0.6, 0.9, and 1.5 cpm/pmol (+Carb). For the +Carb samples, the 3H releases in cycles 6 and 8 can be largely accounted for by the labeling in the desensitized state of δPro-286 and δIle-288 in the contaminating δ subunit fragment. The aligned sequences of the M2−M3 loop and M3 helix of the four nAChR subunits are shown at the top, with bold highlighting for the conserved V8 protease site (E) and the Pro (P) 6 cycles later and for the M3 methionines (M).

pmol (Figure 7B). After treatment with OPA in cycle 6, the primary sequences were those beginning at βThr-273 (I_0 = 11 pmol) and at γThr-276 (I_0 = 13 pmol), with each sample also containing as a contaminating secondary sequence the corresponding δ subunit fragment beginning at δThr-281 (I_0 = 3 pmol). For nAChRs labeled in the desensitized state, the labeling of βMet-288 was reduced by 85% and of γMet-291 by 50%, and the major 3H releases were in cycles 6 and 8. Because of the prominent labeling of δPro-286 and δIle-288 in the desensitized state (Figure 6), the 3H releases seen in cycles 6 and 8 for the β and γ subunit digests can be accounted for by the labeling in the contaminating δ subunit fragment, rather than labeling of the corresponding positions in the β or γ subunits.

Agonist-Independent [3H]BP Photolabeling in αM4. Within the nAChR transmembrane domain, the M4 α-helices have the greatest exposure to lipid (*7*), and amino acids in the M4 helices in contact with lipid have been identified by hydrophobic labeling with [125I]TID (*20*) and [3H]diazofluorene (*17*). We characterized [3H]BP photoincorporation in αM4 by sequencing the α subunit fragment beginning at αTyr-401 that can be isolated by reversed-phase HPLC from tryptic digests of αV8-10 (*20*) (Figure 8 and Supporting Information Figure S3B). The peak of 3H release in cycle 15 indicated labeling of αMet-415, the only Met in αM4 and one of the amino acids labeled by [125I]TID and [3H]-diazofluorene. It was labeled at equal efficiency (4 cpm/pmol) in nAChRs labeled in the absence or presence of agonist and at least 10-fold higher efficiency than any other amino acid in αM4. For comparison, the 3H release in cycle 12 was consistent with labeling of αCys-412 at ~0.4 cpm/pmol.

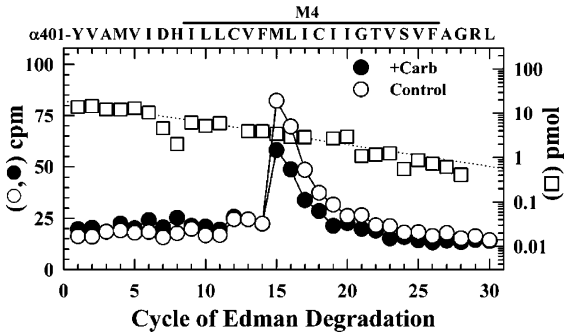

FIGURE 8: Agonist-insensitive [3H]BP photolabeling in αM4. 3H (○, ●) and PTH-amino acids released (□) during sequencing of fragments isolated from trypsin digests of αV8-10, isolated from nAChRs labeled with [3H]BP in the absence (○) or presence (●) of Carb in the photolabeling experiments shown in Figures 6 and 7. The trypsin digests of αV8-10 were fractionated by reversed-phase HPLC, and material in the broad peak of 3H (fractions 27−32, centered at 80% solvent B) was pooled and sequenced. The primary sequence began at αTyr-401 [−Carb (□), I_0 = 17 pmol, R = 89%; +Carb, I_0 = 12 pmol, R = 89%], and the secondary sequence began at αSer-388 (I_0 ~ 2 pmol). The release of 3H in cycle 15 (−Carb, 65 cpm) indicated labeling of αMet-415 at 4 (−Carb) and 3 (+Carb) cpm/pmol. For a parallel sample isolated from nAChRs labeled in the presence of Carb and 100 μM PCP, αMet-415 was also labeled at 4 cpm/pmol.

DISCUSSION

In this work we used [3H]BP as a hydrophobic photoprobe to provide novel information about the regions of the nAChR transmembrane domain that differ in structure between the resting and desensitized states. BP interacts with only low affinity with the nAChR, as judged by the IC_{50}'s of 150 and 600 μM characterizing BP inhibition of [3H]tetracaine binding and ACh current responses, respectively, or the even higher concentrations necessary to inhibit [3H]PCP binding. Nevertheless, for nAChRs equilibrated with [3H]BP at a low concentration (0.3 μM), our photolabeling results establish that BP binds at multiple sites within the nAChR transmembrane domain. Localization of the photolabeled amino acids in the available nAChR structural model (*8*), which is shown in Figure 9 and discussed in more detail later, establishes that BP can bind (i) within the ion channel at the level of M2-13 and M2-9, (ii) in the δ subunit at the interface with the extracellular domain (δPhe-232 in δM1 and δPro-286/δIle-288 within the δM2−M3 loop), (iii) at the $\beta-\alpha$ and $\gamma-\alpha$ subunit interfaces (βMet-288 and γMet-291 in the M3 helices), and (iv) at the lipid interface (αMet-415 in αM4, the only M4 segment characterized). While the labeling at

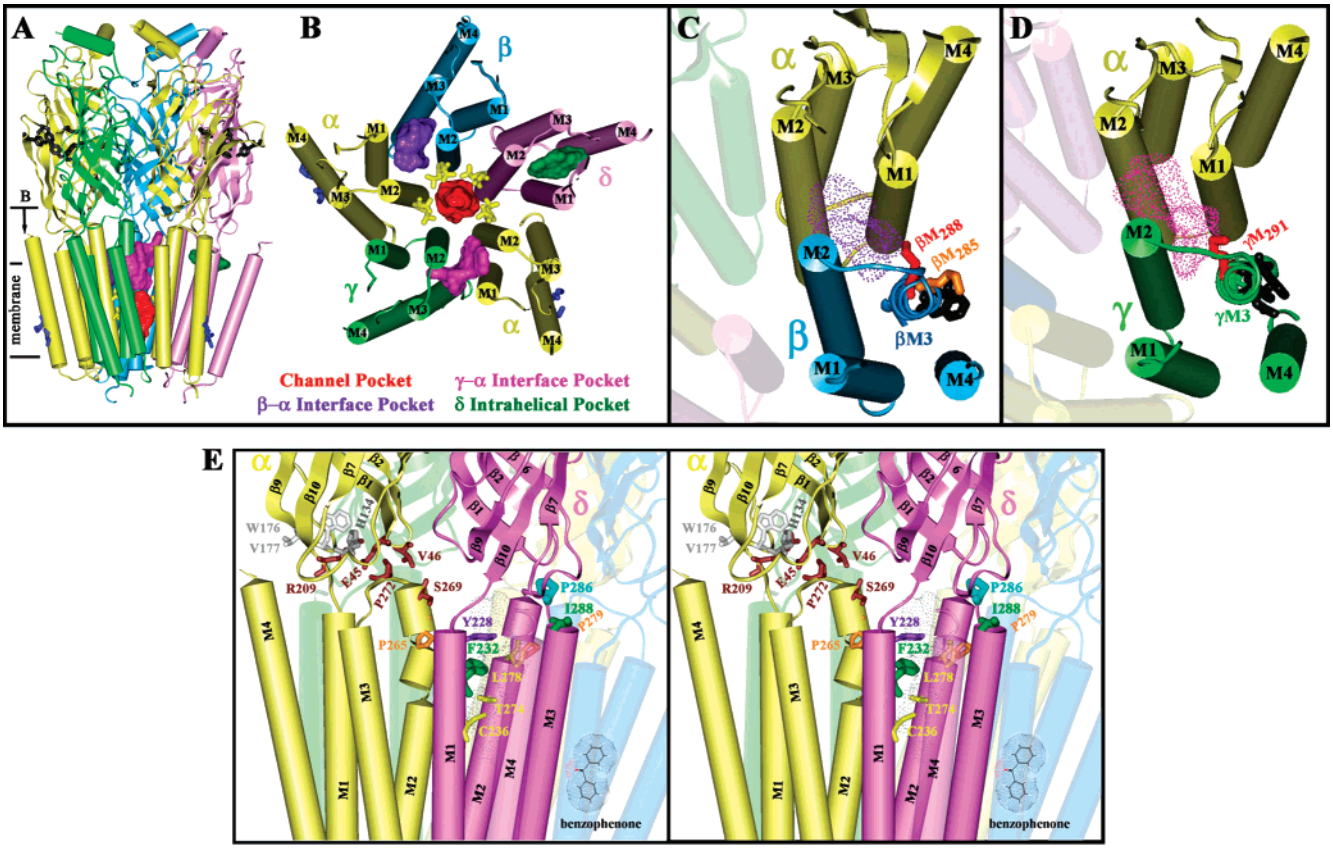

FIGURE 9: The binding sites for BP in the *Torpedo* nAChR transmembrane domain. A molecular model of the *Torpedo* nAChR (PDB code 2BG9) represented by secondary structure elements (α-helices as cylinders and *β*-sheets as ribbons) is shown in multiple views to highlight the different BP binding sites. (A) The nAChR in side view, with the cytoplasmic helices omitted. Included in stick representation are the aromatic side chains of the ACh binding sites. (B) A view from the perspective indicated by the arrow in (A) of the nAChR transmembrane domain. Included in stick representation are the residues labeled by [^{3}H]BP in the channel (yellow, M2-13′ and M2-9′) or at the lipid−protein interface (blue, αM4 Met-415 and Cys-412). Connolly surfaces of docked BPs (see Experimental Procedures) are included for the four state-dependent binding pockets identified by photolabeling. (C, D) Views of the transmembrane domain looking down the axes of the *β*M3 (C) and *γ*M3 (D) helices. In stick representation are the M3 residues labeled by [^{125}I]TID from the lipid−protein interface [black (*20*)], by [^{3}H]BP (red), or by both (orange). The pockets defined by BP docking are included as dotted Connolly surfaces. (E) A stereo representation highlighting the pocket within the *δ* subunit transmembrane domain with the amino acids identified that are labeled by [^{3}H]BP selectively in the desensitized state (cyan and green) and/or by [^{125}I]TID in the open state [yellow and green (*18*)]. *δ*Tyr-228, which is labeled by halothane in the desensitized state, is shown in purple (*44*). The amino acids in the α subunit extracellular domain reported to be labeled by BP in the mouse nAChR are included [gray (*27*)] as are the residues identified by mutational analyses to be involved in coupling agonist binding to channel activation [brown (*12*)]. The conserved prolines (orange) that break the M2 helices at the synaptic end are shown along with their helical breaks. The water-accessible space within the *δ* subunit helix bundle identified by the PASS program (Experimental Procedures) is included as a dotted Connolly surface, and the structure of BP is included for scale.

Table 1: State Dependence of [^{3}H]BP Photoincorporation into Residues in the nAChR Transmembrane Domain (cpm/pmol of PTH Derivative)[a]

amino acid	−Carb	+Carb	amino acid	−Carb	+Carb	amino acid	−Carb	+Carb
	αM2			*β*M2			δM2	
αLeu-251	2	ND	*β*Leu-257	3	0.1	δLeu-265	1.5 ± 0.3	4 ± 1
αVal-255	10	ND	*β*Val-261	16	3	δVal-269	38 ± 4	14 ± 4
	*β*M3			*γ*M3			δM3	
*β*Met-285	2	0.6				δMet-293	0.7 ± 0.1	<0.5
*β*Met-288	5	0.9	*γ*Met-291	2.9	1.5	δMet-296	0.5 ± 0.5	<0.5
	δM1			δM2−M3 loop			αM4	
δTyr-228	<0.2	1 ± 0.2	δPro-286	0.3 ± 0.3	5 ± 1	αCys-412	0.4	0.4
δPhe-232	0.7 ± 0.1	5 ± 2	δIle-288	0.1 ± 0.1	5 ± 1	αMet-415	4	3

[a] The ^{3}H incorporation in each residue was calculated from the observed ^{3}H release as described under Experimental Procedures, and the mass was calculated from the initial and repetitive yields. The results are from a single photolabeling experiment, including data from Figures 6−8. When sufficient material was available for two aliquots to be sequenced, the data are presented as the mean and range. ND, not determined.

the lipid interface was the same in the resting and desensitized states, labeling in the ion channel was reduced by 90% in the desensitized state, and the labeling of δPhe-232/δPro-286/δIle-288 occurred only in the desensitized state.

Table 1 summarizes, for comparison purposes, the efficiencies of [^{3}H]BP photoincorporation in the amino acids in these different structural domains from one of the labeling experiments. For the nAChR equilibrated with 0.3 *μ*M [^{3}H]-

BP in the absence of agonist, the amino acid labeled most efficiently was δVal-269 within the ion channel, which was labeled at ~0.1% efficiency (40 cpm/pmol); the labeling efficiency of Met in βM3, γM3, and αM4 was ~0.01%; and that of αCys-412 in αM4 was ~0.001%. Although in the desensitized state the observed labeling efficiency of δVal-269 (14 cpm/pmol) was similar to that of δPhe-232/δPro-286/δIle-288 (each at 5 cpm/pmol), as discussed in the footnotes 2 and 3, the chemical instability of BP adducts with δPhe-232 and δPro-286 causes those labeling efficiencies to be substantially underestimated. Since the pharmacological assays indicate that BP has only low-affinity interactions with the nAChR, we expect that the observed low efficiency photolabeling occurs in large measure because of low fractional occupancy at each of the sites and that the efficiency of photolabeling of δVal-269 and each of the other labeled amino acids will increase linearly with BP concentration at least up to 100 μM.

BP as a Probe of State-Dependent Changes in the nAChR Transmembrane Domain. The amino acids photolabeled by [^{3}H]BP are identified in Figure 9 in the model of the structure of the *Torpedo* nAChR in the absence of agonist (PDB code 2BG9). Amino acids labeled within the M2 ion channel domain and at the lipid interface (αM4) are shown in Figure 9B; those labeled in βM3 and γM3 are identified in Figure 9C,D; and the amino acids in δM1 and in the δM2−M3 loop are shown in stereo in Figure 9E. Also depicted in Figure 9A,B are the Connolly surface representations of the predicted binding pockets for BP within the nAChR transmembrane domain in the lumen of the channel, the δ subunit four-helix bundle, and at the γ−α and β−α subunit interfaces (see Experimental Procedures).

The labeling in the desensitized state and absence of labeling in the resting state of δPhe-232 in δM1 and of δPro-286/δIle-288 in the M2−M3 loop provide clear evidence of an agonist-induced change in structure in this region of the δ subunit that is also in contact with amino acids in the extracellular domain. Although in the closed state structure δPro-286 is oriented toward the extracellular domain and the side chain of δIle-288 is oriented away from the pocket containing δPhe-232, only subtle structural rearrangements are required to reorient those amino acids toward this pocket. However, it is striking that in the closed state structure the shortest distances from δPhe-232 to δPro-286 and δIle-288 are 15−18 Å, i.e., substantially greater than the 8 Å maximal length of BP. Although the docking calculations predict a preferred positioning of BP stacked between the aromatic rings of δTyr-228 and δPhe-232, the absence of labeling of those side chains in the absence of agonist suggests that a compact binding pocket in this region does not exist in the closed state. It is plausible that the agonist-induced change in structure involves a reorganization of the M2−M3 loop that brings δPro-286 and δIle-288 in closer proximity to δPhe-232, forming such a binding pocket. This reorganization would also require a reorientation of the extracellular end of M2, presumably associated with a break of the helix at δPro-279. Since we found no evidence of labeling of amino acids at the base of the δ subunit extracellular domain, which are all contained within δEKC-21 (beginning at δHis-26/δGlu-47), there is no evidence that the labeling of δPro-286/δIle-288 results from BP binding between those amino acids and amino acids in the extracellular domain.

Interestingly, αPro-272, the position in the α subunit equivalent to δPro-286, has been identified by mutational analyses as a position crucial in the link between agonist binding and channel gating that interacts energetically with αGlu-45 and αVal-46 at the base of the extracellular domain (*12*). Within the serotonin 5-HT$_3$ receptor, a homopentamer, agonist-dependent conformational transitions have been proposed to involve the cis−trans isomerization of the equivalent proline (5-HT$_3$R αPro-308) (*43*). Although we were unable to cleave the α subunit at αGlu-262 to test directly for labeling of αPro-272, in contrast to the δ subunit, there was no evidence of prominent labeling within the α subunit in the desensitized state.

Selective labeling of δIle-288 was reported for [^{125}I]TID in the open state compared to the closed or desensitized state, and the open state labeling of this residue along with residues in δM1 (δPhe-232 and δCys-236) and δM2 (δThr-274 and δLeu-278) provided evidence for the formation in the open state of a hydrophobic pocket between δM1, δM2, and δM3 (*18*). While [^{3}H]BP photolabeled δPhe-232 and δIle-288 in the desensitized state, the labeling of δPro-286 and the lack of labeling of δThr-274 and δLeu-278 indicate that BP is not photolabeling in the desensitized state the same structure as that labeled by [^{125}I]TID in the open state. [^{3}H]BP photolabeling of nAChRs frozen in the open state will be necessary to provide a direct comparison of changes in structure in this region between the open and desensitized states.

The agonist-inhibitable labeling in the ion channel domain at M2-13 is qualitatively similar to that seen for [^{125}I]TID (*16*) and [^{3}H]diazofluorene (*17*). Although the reactive carbene intermediates formed upon photolysis of TID or diazofluorene react efficiently with water, the reactive ketyl diradical of BP does not (*21*). Thus, the presence of water in the channel in the desensitized state would not act as a quencher of BP labeling, and the reduction of labeling in the desensitized state seen for the three ligands results from a change in the structure of the channel domain unrelated to changes in solvation.

[^{3}H]BP photolabeling in αM4 of αMet-415 (and αCys-412 at lower efficiency), which were also labeled by [^{125}I]-TID and [^{3}H]diazofluorene (*17*), was the same in the absence and presence of agonist, and labeling was also unaffected by tetracaine. Thus, the labeling of these residues is as expected for amino acids at the lipid interface (Figure 9B). In contrast, the labeling in βM3 and γM3 of βMet-288 and γMet-291 was reduced by 85% and 50% in the desensitized state. While [^{125}I]TID labeled nonspecifically other residues in βM3 (βMet-285, βIle-289, and βPhe-293) and γM3 (γPhe-292, γLeu-296, γMet-299, and γAsn-300), it did not label βMet-288 or γMet-291 (*20*). Inspection of Figure 9C,D reveals that the [^{3}H]BP-labeled βMet-288 and γMet-291 lie on the surface of the M3 helices ~100° from the surfaces defined by [^{125}I]TID labeling and that the [^{3}H]BP-labeled residues are both oriented toward an αM1 helix rather than lipid. Thus, the agonist-sensitive labeling of βMet-288 and γMet-291 by [^{3}H]BP reveals a change in structure between the resting and desensitized states at the β−α and γ−α subunit interfaces in the transmembrane domain. Although we were unable to generate the cleavage in the α subunit M2−M3 loop necessary to characterize labeling in αM3,

no labeling was seen of δMet-296, the position equivalent to βMet-288 or γMet-291, or of other amino acids in δM3.

Side-Chain Selectivity of BP Photolabeling. BP-based photoaffinity probes have been shown to incorporate into a wide variety of amino acids (*22*), but studies with N-acylated amino acid esters reveal strong side chain and solvent dependencies (*23*). Recent studies with peptide GPCRs reveal a strong preference for reaction with Met in the peptide binding sites (*24*−*26*). The labeling of αMet-415 in αM4 and of βMet-288 and γMet-291 in the M3 helices indicates that BP also reacts preferentially with that side chain in hydrophobic environments. BP did not, however, photolabel the Met at the N-termini of the M2 helices or αMet-404, which in the nAChR structure are predicted to be exposed at the cytoplasmic surface. The labeling of Leu and Val in the M2 ion channel domain at M2-9 and M2-13 and of δPhe-232 in δM1 and δPro-286/δIle-288 near the N-terminus of δM3 occurs in regions of nAChR structure where there are no methionines.

BP Photolabeling in the nAChR Extracellular Domain? In our studies of *Torpedo* nAChR photolabeled with [^{3}H]-BP at 0.3 μM, we found photolabeling restricted to the nAChR transmembrane domain, with less than 2% of α or δ subunit labeling recovered in αV8-18 (beginning at αThr-52) or δEKC-21 (beginning at δHis-26/δGlu-47), based upon the ^{3}H incorporation in HPLC-purified subunit fragments. This contrasts with a recent report (*27*) of oocyte-expressed mouse nAChRs photolabeled with 10 μM BP, where photolabeling was reported of amino acids in the extracellular domain [αHis-134 (within αV8-18) and αThr-196 (within αV8-20) in the resting state and αArg-340 in the cytoplasmic M3−M4 loop (in αV8-10) in the desensitized state]. Since the detection of hydrophobic, membrane spanning segments remains challenging and unreliable for current LC/MS techniques, we are not surprised that we were able to identify labeling in the nAChR transmembrane domain that eluded detection by LC/MS, and the level of ^{3}H incorporation in αV8-18 or δEKC-21 is consistent with labeling of one or a few amino acids at ∼1 cpm/pmol. Interestingly, the amino acids of the extracellular domain predicted to be in proximity with δPro-286 (δGlu-47/Thr-48) are within δEKC-21, but those in proximity to αPro-272 (αGlu-45/Val-46) are within αV8-4, which begins at Ser-1 (*31*). BP-based photoprobes can incorporate into amino acids in the *Torpedo* nAChR extracellular domain, as evidenced by the efficient labeling of γLeu-109/δLeu-111 in the ACh binding sites by [^{3}H]-benzoylbenzoylcholine (*18*), but further studies will be necessary to determine whether there is [^{3}H]BP photolabeling of any amino acids in the extracellular domain.

SUPPORTING INFORMATION AVAILABLE

Three figures as described in the text. This material is available free of charge via the Internet at http://pubs.acs.org.

REFERENCES

1. Corringer, P.-J., Le Novere, N., and Changeux, J.-P. (2000) Nicotinic receptors at the amino acid level, *Annu. Rev. Pharmacol. Toxicol. 40*, 431−458.
2. Lynch, J. W. (2004) Molecular structure and function of the glycine receptor chloride channel, *Physiol. Rev. 84*, 1051−1095.
3. Sine, S. M., and Engel, A. G. (2006) Recent advances in Cys-loop receptor structure and function, *Nature 440*, 448−455.
4. Brejc, K., van Dijk, W. J., Klaassen, R., Schuurmans, M., van der Oost, J., Smit, A. B., and Sixma, T. K. (2001) Crystal structure of AChBP reveals the ligand-binding domain of nicotinic receptors, *Nature 411*, 269−276.
5. Celie, P. H. N., van Rossum-Fikkert, S. E., van Dijk, W. J., Brejc, K., Smit, A. B., and Sixma, T. K. (2004) Nicotinic and carbamylcholine binding to nicotinic acetylcholine receptors as studied in AChBP crystal structures, *Neuron 41*, 907−914.
6. Hansen, S. B., Sulzenbacher, G., Huxford, T., Marchot, P., Taylor, P., and Bourne, Y. (2005) Structures of *Aplysia* AChBP complexes with nicotinic agonists and antagonists reveal distinctive binding interfaces and conformations, *EMBO J. 24*, 3635−3646.
7. Miyazawa, A., Fujiyoshi, Y., and Unwin, N. (2003) Structure and gating mechanism of the acetylcholine receptor pore, *Nature 423*, 949−958.
8. Unwin, N. (2005) Refined structure of the nicotinic acetylcholine receptor at 4 Å resolution, *J. Mol. Biol. 346*, 967−989.
9. Wilson, G. G., and Karlin, A. (2001) Acetylcholine receptor channel structure in the resting, open, and desensitized states probed with the substituted-cysteine-accessibility method, *Proc Natl. Acad. Sci. U.S.A. 98*, 1241−1248.
10. Kash, T. L., Jenkins, A., Kelley, J. C., Trudell, J. R., and Harrison, N. L. (2003) Coupling of agonist binding to channel gating in the $GABA_A$ receptor, *Nature 421*, 272−275.
11. Bouzat, C., Gumilar, F., Spitzmaul, G., Wang, H. L., Rayes, D., Hansen, S. B., Taylor, P., and Sine, S. M. (2004) Coupling of agonist binding to channel gating in an ACh-binding protein linked to an ion channel, *Nature 430*, 896−900.
12. Lee, W. Y., and Sine, S. M. (2005) Principal pathway coupling agonist binding to channel gating in nicotinic receptors, *Nature 438*, 243−247.
13. Xiu, X. N., Hanek, A. P., Wang, J. T., Lester, H. A., and Dougherty, D. A. (2005) A unified view of the role of electrostatic interactions in modulating the gating of Cys loop receptors, *J. Biol. Chem. 280*, 41655−41666.
14. Grosman, C., Zhou, M., and Auerbach, A. (2000) Mapping the conformational wave of acetylcholine receptor channel gating, *Nature 403*, 773−776.
15. Chakrapani, S., Bailey, T. D., and Auerbach, A. (2004) Gating dynamics of the acetylcholine receptor extracellular domain, *J. Gen. Physiol. 123*, 341−356.
16. White, B. H., and Cohen, J. B. (1992) Agonist-induced changes in the structure of the acetylcholine receptor M2 regions revealed by photoincorporation of an uncharged nicotinic non-competitive antagonist, *J. Biol. Chem. 267*, 15770−15783.
17. Blanton, M. P., Dangott, L. J., Raja, S. K., Lala, A. K., and Cohen, J. B. (1998) Probing the structure of the nicotinic acetylcholine receptor ion channel with the uncharged photoactivable compound [^{3}H]diazofluorene, *J. Biol. Chem. 273*, 8659−8668.
18. Arevalo, E., Chiara, D. C., Forman, S. A., Cohen, J. B., and Miller, K. W. (2005) Gating-enhanced accessibility of hydrophobic sites within the transmembrane region of the nicotinic acetylcholine receptor's delta- subunit-A time-resolved photolabeling study, *J. Biol. Chem. 280*, 13631−13640.
19. Mourot, A., Grutter, T., Goeldner, M., and Kotzyba-Hibert, F. (2006) Dynamic structural investigations on the Torpedo nicotinic acetylcholine receptor by time-resolved photoaffinity labeling, *ChemBioChem 7*, 570−583.
20. Blanton, M. P., and Cohen, J. B. (1994) Identifying the lipid-protein interface of the *Torpedo* nicotinic acetylcholine receptor: secondary structure implications, *Biochemistry 33*, 2859−2872.
21. Dorman, G., and Prestwich, G. D. (1994) Benzophenone photophores in biochemistry, *Biochemistry 33*, 5661−5673.
22. Kotzyba-Hibert, F., Kapfer, I., and Goeldner, M. (1995) Recent trends in photoaffinity labeling, *Angew. Chem., Int. Ed. 34*, 1296−1312.
23. Deseke, E., Nakatani, Y., and Ourisson, G. Intrinsic reactivities of amino acids towards photoalkylation with benzophenone; a study preliminary to photolabeling of the transmembrane protein Glycophorin A, *Eur. J. Org. Chem. 1998*, 243−251.
24. Macdonald, D., Mierke, D. F., Li, H. Z., Pellegrini, M., Sachais, B., Krause, J. E., Leeman, S. E., and Boyd, N. D. (2001) Photoaffinity labeling of mutant neurokinin-1 receptors reveals additional structural features of the substance P/NK-1 receptor complex, *Biochemistry 40*, 2530−2539.
25. Clement, M., Martin, S. S., Beaulieu, M. E., Chamberland, C., Lavigne, P., Leduc, R., Guillemette, G., and Escher, E. (2005) Determining the environment of the ligand binding pocket of the

human angiotensin II type I (HAT(1)) receptor using the methionine proximity assay, *J. Biol. Chem. 280*, 27121−27129.
26. Wittelsberger, A., Thomas, B. E., Mierke, D. F., and Rosenblatt, M. (2006) Methionine acts as a "magnet" in photoaffinity crosslinking experiments, *FEBS Lett. 580*, 1872−1876.
27. Leite, J. F., Blanton, M. P., Shahgholi, M., Dougherty, D. A., and Lester, H. A. (2003) Conformation-dependent hydrophobic photolabeling of the nicotinic receptor: Electrophysiology-coordinated photochemistry and mass spectrometry, *Proc. Natl. Acad. Sci. U.S.A. 100*, 13054−13059.
28. Middleton, R. E., and Cohen, J. B. (1991) Mapping of the acetylcholine binding site of the nicotinic acetylcholine receptor: [3H]-nicotine as an agonist photoaffinity label, *Biochemistry 30*, 6987−6997.
29. Chiara, D. C., Xie, Y., and Cohen, J. B. (1999) Structure of the agonist-binding sites of the Torpedo nicotinic acetylcholine receptor: Affinity-labeling and mutational analyses identify gamma Tyr-111/delta Arg-113 as antagonist affinity determinants, *Biochemistry 38*, 6689−6698.
30. White, B. H., Howard, S., Cohen, S. G., and Cohen, J. B. (1991) The hydrophobic photoreagent 3-(trifluoromethyl)-3-(*m*-[125I]-iodophenyl)diazirine is a novel noncompetitive antagonist of the nicotinic acetylcholine receptor, *J. Biol. Chem. 266*, 21595−21607.
31. White, B. H., and Cohen, J. B. (1988) Photolabeling of membrane-bound *Torpedo* nicotinic acetylcholine receptor with the hydrophobic probe 3-trifluoromethyl-3-(*m*-[125I]iodophenyl)diazirine, *Biochemistry 27*, 8741−8751.
32. Schagger, H., and von Jagow, G. (1987) Tricine-sodium dodecyl sulfate-polyacrylamide gel electrophoresis for the separation of proteins in the range from 1 to 100 kDa, *Anal. Biochem. 166*, 368−379.
33. Brauer, A. W., Oman, C. L., and Margolies, M. N. (1984) Use of *o*-phthalaldehyde to reduce background during automated Edman degradation, *Anal. Biochem. 137*, 134−142.
34. Brady, G. P., and Stouten, P. F. W. (2000) Fast prediction and visualization of protein binding pockets with PASS, *J. Comp. Mol. Des. 14*, 383−401.
35. Middleton, R. E., Strnad, N. P., and Cohen, J. B. (1999) Photoaffinity labeling the *torpedo* nicotinic acetylcholine receptor with [3H]tetracaine, a nondesensitizing noncompetitive antagonist, *Mol. Pharmacol. 56*, 290−299.
36. Oswald, R. E., Heidmann, T., and Changeux, J.-P. (1983) Multiple affinity sites for noncompetitive blockers revealed by [3H]-phencyclidine binding to acetylcholine receptor rich membrane fragments from *Torpedo marmorata*, *Biochemistry 22*, 3128−3136.
37. Wu, G., Raines, D. E., and Miller, K. W. (1994) A hydrophobic inhibitor of the nicotinic acetylcholine receptor acts on the resting state, *Biochemistry 33*, 15375−15381.
38. Gallagher, M. J., and Cohen, J. B. (1999) Identification of amino acids of the *torpedo* nicotinic acetylcholine receptor contributing to the binding site for the noncompetitive antagonist [3H]tetracaine, *Mol. Pharmacol. 56*, 300−307.
39. Boyd, N. D., and Cohen, J. B. (1984) Desensitization of membrane-bound *Torpedo* acetylcholine receptor by amine noncompetitive antagonists and aliphatic alcohols: studies of [3H]-acetylcholine binding and $^{22}Na^{+}$ ion fluxes, *Biochemistry 23*, 4023−4033.
40. Gallagher, M. J., Chiara, D. C., and Cohen, J. B. (2001) Interactions between 3-(trifluoromethyl)-3-(*m*-[125I]iodophenyl)-diazirine and tetracaine, phencyclidine, or histrionicotoxin in the *Torpedo* nicotinic acetylcholine receptor ion channel, *Mol. Pharmacol. 59*, 1514−1522.
41. Pedersen, S. E., Sharp, S. D., Liu, W.-S., and Cohen, J. B. (1992) Structure of the noncompetitive antagonist binding site in the *Torpedo* nicotinic acetylcholine receptor: [3H]Meproadifen mustard reacts selectively with α-subunit Glu-262, *J. Biol. Chem. 267*, 10489−10499.
42. Pratt, M. B., Husain, S. S., Miller, K. W., and Cohen, J. B. (2000) Identification of sites of incorporation in the nicotinic acetylcholine receptor of a photoactivatible general anesthetic, *J. Biol. Chem. 275*, 29441−29451.
43. Lummis, S. C. R., Beene, D. L., Lee, L. W., Lester, H. A., Broadhurst, R. W., and Dougherty, D. A. (2005) Cis-trans isomerization at a proline opens the pore of a neurotransmitter-gated ion channel, *Nature 438*, 248−252.
44. Chiara, D. C., Dangott, L. J., Eckenhoff, R. G., and Cohen, J. B. (2003) Identification of nicotinic acetylcholine receptor amino acids photolabeled by the volatile anesthetic halothane, *Biochemistry 42*, 13457−13467.
45. Cole, D. G. and Yount, R. G. (1990) Photolabeling of the 6 and 10 S conformationsof gizzard myosin with 3′(2′)-*O*-(4-Benzoyl)-benzoyl-ATP, *J. Biol. Chem. 265*, 22537−22546.

BI7008163